Received: 6 March 2019 | Revised: 20 May 2019 | Accepted: 9 July 2019

DOI: 10.1002/jbio.201900086

FULL ARTICLE

JOURNAL OF BIOPHOTONICS

Imaging depth variations in hyperspectral imaging: Development of a method to detect tumor up to the required tumor-free margin width

Esther Kho[1]* | Lisanne L. de Boer[1] | Anouk L. Post[1,2] | Koen K. Van de Vijver[3,4] | Katarzyna Jóźwiak[5] | Henricus J.C.M. Sterenborg[1,2] | Theo J.M. Ruers[1,6]

[1]Department of Surgery, the Netherlands Cancer Institute, Amsterdam, the Netherlands

[2]Department of Biomedical Engineering and Physics, Amsterdam University Medical Center, Amsterdam, the Netherlands

[3]Department of Pathology, the Netherlands Cancer Institute, Amsterdam, the Netherlands

[4]Department of Pathology, Ghent University Hospital, Ghent, Belgium

[5]Department of Epidemiology and Biostatistics, the Netherlands Cancer Institute, Amsterdam, the Netherlands

[6]Faculty of Science and Technology, University of Twente, Enschede, the Netherlands

***Correspondence**
Esther Kho, Department of Surgery, the Netherlands Cancer Institute, Plesmanlaan 121, 1066 CX, Amsterdam, the Netherlands.
Email: e.kho@nki.nl

Funding information
KWF Kankerbestrijding, Grant/Award Number: grant KWF 10747

Abstract

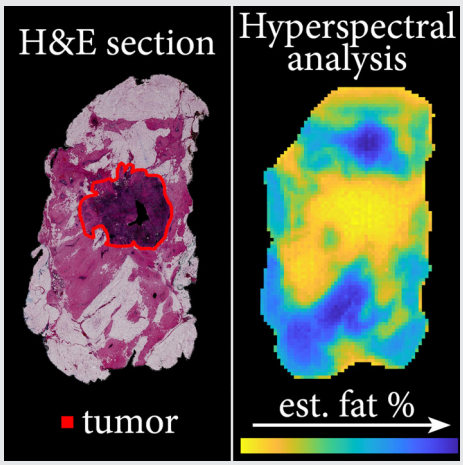

Hyperspectral imaging is a promising technique for resection margin assessment during cancer surgery. Thereby, only a specific amount of the tissue below the resection surface, the clinically defined margin width, should be assessed. Since the imaging depth of hyperspectral imaging varies with wavelength and tissue composition, this can have consequences for the clinical use of hyperspectral imaging as margin assessment technique. In this study, a method was developed that allows for hyperspectral analysis of resection margins in breast cancer. This method uses the spectral slope of the diffuse reflectance spectrum at wavelength regions where the imaging depth in tumor and healthy tissue is equal. Thereby, tumor can be discriminated from healthy breast tissue while imaging up to a similar depth as the required tumor-free margin width of 2 mm. Applying this method to hyperspectral images acquired during surgery would allow for robust margin assessment of resected specimens. In this paper, we focused on breast cancer, but the same approach can be applied to develop a method for other types of cancer.

KEYWORDS

breast-conserving surgery, diffuse reflectance, hyperspectral imaging depth, penetration depth, resection margin assessment, resection margin width

1 | INTRODUCTION

Surgery is usually the preferred treatment for patients with cancer. Thereby, surgeons aim to remove the tumor with a surrounding margin of normal tissue, while sparing as much healthy tissue as possible. However, since tumor tissue is difficult to distinguish by eye, complete tumor removal remains challenging [1–3]. Completeness of tumor removal is determined by a pathologist, who examines the resection margin under a microscope. For cancer surgery in

which large specimens are excised, histopathologic evaluation of the whole margin is too time-consuming to be performed during surgery and typically requires several days. If a tumor-positive margin is found, often additional treatment like a second surgical procedure or radiation therapy is needed.

Hyperspectral imaging is a non-invasive and rapid technique for the examination of the resection margins during surgery. As the entire surface of a resected specimen can be imaged fast and hyperspectral diffuse reflectance measurements can be analyzed directly, tumor-positive margins can be found during the initial surgery in order to excise remaining tumor tissue in the patient immediately [4]. Previous research showed promising results in detecting tumor tissue in resected specimens with hyperspectral imaging [5–9]. Importantly, for hyperspectral imaging as margin assessment technique, the imaging depth should be taken into account. Ideally, the imaging depth should equal the required tumor-free margin width to remove the whole tumor while sparing as much healthy tissue as possible. The tumor-free margin width is in the order of millimeters and depends on the type of cancer and the guidelines of a country [1–3, 8].

With hyperspectral imaging, each pixel in the image contains an entire spectrum over a broad wavelength range. As the optical penetration depth varies with tissue composition and wavelength, different wavelengths sample different tissue volumes with hyperspectral imaging [4, 10, 11]. Therefore, a tumor that is located a few millimeters underneath the resection surface might be detected by wavelengths that have a larger penetration depth and be missed by wavelengths with superficial penetration depth. When hyperspectral data analysis is performed on the entire spectrum, these differences in sampling volume are not taken into account. Therefore, in previous research, the optical parameters of skin were obtained by applying a two-layered model on separate wavelength ranges in the hyperspectral data where the penetration depth was assumed more or less uniform [12].

In this study, we developed a method that allows for hyperspectral margin assessment, with an imaging depth similar to the required tumor-free margin width. We focussed on breast cancer, but the same approach can be applied to other types of cancer as well. For breast cancer, the American guideline requires a tumor-free margin width up to 2 mm [3]. Therefore, hyperspectral imaging should be able to assess tissue up to a depth of 2 mm below the resection surface. To develop this method, we first identified wavelength regions at which the penetration depth of photons does not depend on whether the tissue is healthy or malignant. Previous research showed that the amount of water and fat is one of the main optical differences between tumor and healthy breast tissue [13–20]. Therefore, we focused on the near-infrared wavelength range, where water and fat are the main absorbers. Second, we used diffusion theory to estimate the theoretical optical penetration depth at these wavelengths. We compared this penetration depth to the imaging depth of our setup, which we determined experimentally using a tissue-mimicking phantom. Third, we estimated the penetration depth in human breast tissue and developed a method using the selected wavelength regions to discriminate between healthy and tumor tissue. Finally, we applied this method to ex vivo breast samples and show that it can discriminate between healthy and tumor tissue.

2 | MATERIALS AND METHODS

2.1 | Hyperspectral imaging setup

Hyperspectral images were acquired with two pushbroom hyperspectral imaging systems (LabScanner Setup 40 × 20, Specim, Spectral Imaging Ltd., Finland) that operate in the visual (VIS) and near-infrared (NIR) wavelength range and were controlled by LUMO software (v2016-427, Specim, Spectral Imaging Ltd., Finland). Figure 1 shows the hyperspectral imaging setup. Images acquired with the VIS camera (PFD-CL-65-V10E, CMOS sensor with 1312 × 384 pixels) and the NIR camera (VLNIR CL-350-N17E, InGaAs sensor with 320 × 256 pixels) have a spatial resolution of respectively 0.16 and 0.5 mm/pixel. The material under investigation was placed on a translation stage, illuminated by three halogen light sources (2900 K), and scanned line-by-line by moving the translation stage. The scanning speed for both cameras was adjusted to match the cameras spatial resolution of the imaged line. After excluding the noisy edges of the wavelength range of both cameras, a spectrum between 450 and 1646 was obtained (VIS camera: 450-950 nm, 318 wavelength bands, 3 nm (FWHM) nominal spectral resolution; NIR camera: 953-1646 nm, 210 wavelength bands, 5 nm (FWHM) nominal spectral resolution). The two cameras had different lenses (VIS: OLE 18.5 mm, NIR: OLES15, Specim, Spectral Imaging Ltd., Finland) optimized for the wavelength range of each camera. Both spectral and spatial aberrations are sub-pixel.

Raw hyperspectral data obtained on tissue was normalized to a diffuse reflectance percentage relative to Spectralon (SRT-99-100, Lapsphere, Inc., Northern Sutton, New Hampshire). Prior to this preprocessing step, we corrected for the slight non-linearity of the InGaAs sensor. A detailed description of this preprocessing was described previously [7].

2.2 | Theoretical penetration depth in breast tissue

To allow for hyperspectral analysis of breast tissue at predefined imaging depths, suitable wavelength regions

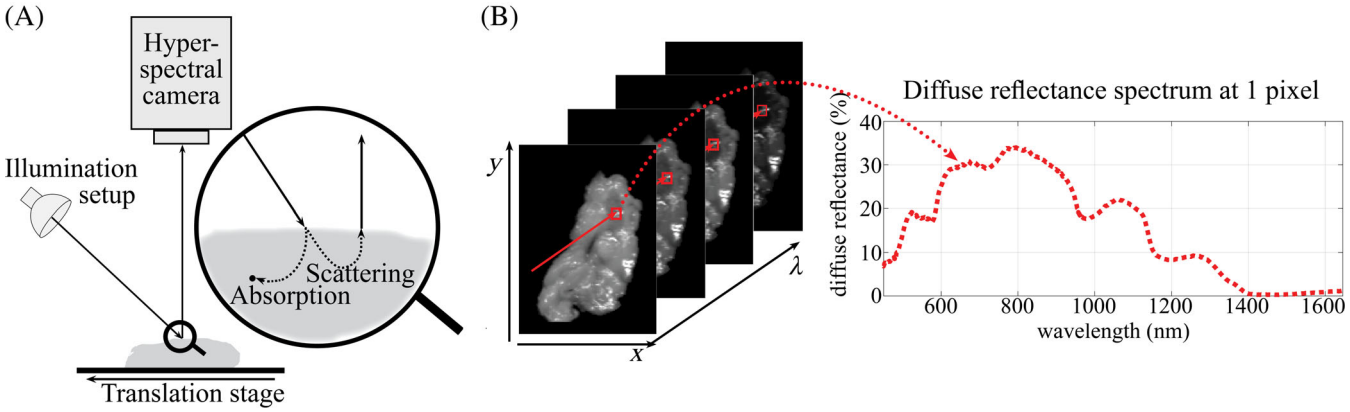

FIGURE 1 (A) Schematic view of the hyperspectral imaging setup. The material under investigation was placed upon a translation stage and illuminated by three halogen light sources under an angle of 45°. By imaging line-by-line, a 3D hypercube (B) was created. All pixels in this hypercube contain multiple 2D images at different wavelengths. By combining both hyperspectral cameras, a diffuse reflectance spectrum between 450 and 1646 nm was obtained

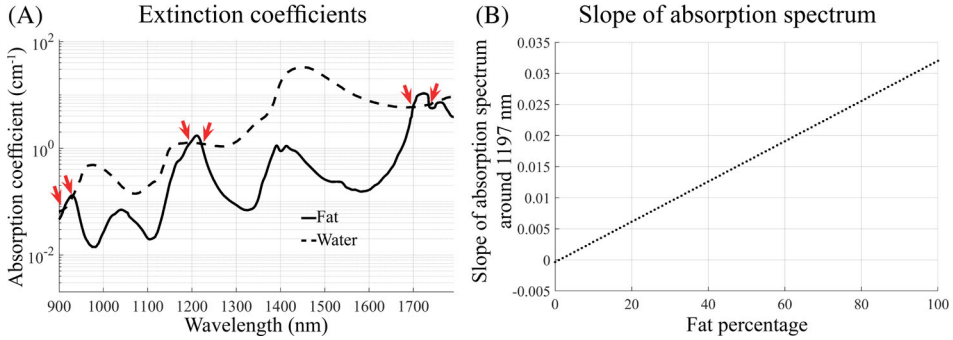

FIGURE 2 (A) The extinction coefficient of water and fat, the main chromophores in the NIR wavelength range. The arrows indicate the isobestic points of the absorption spectra of water and fat: 910, 931, 1197, 1222, 1699 and 1735 nm. (B) The slope of the absorption spectrum for different amounts of water and fat, at the isosbestic point 1197 nm

should be selected that meet the following requirements: First, the penetration depth at these wavelengths should not depend on whether tumor or healthy tissue is imaged. Second, the penetration depth should be clinically relevant for margin assessment, with 2 mm for breast-conserving surgery.

2.2.1 | Equal penetration depth in healthy and tumor breast tissue: isosbestic points

Based on previous research, one of the main differences in optical properties between tumor and healthy breast tissue is the higher water and lower fat content in tumors compared to healthy tissue [13–20]. Therefore, we focused on the NIR wavelength range, where water and fat are the main absorbers of light.

The optical penetration depth varies with tissue composition and wavelength and is depended on the absorption and scattering of light in tissue. In the NIR, the reduced scattering is dominated by Mie scattering. Since this type of scattering gradually decreases with wavelength, it is, in comparison to the absorption, not strongly wavelength dependent. Therefore, the optical penetration depth in the NIR will mainly vary due to differences in absorption. By selecting wavelength regions at which the absorption of light in tumor and healthy tissue is similar, the penetration depth in both tissue types will be the same. In the NIR, these regions are at the isosbestic points of the absorption spectra of water and fat (Figure 2A) [21]. Due to the equal absorption of water and fat, the reflectance at these points will likely be the same for healthy and malignant tissue. However, at these wavelengths, the slope of the absorption spectrum is strongly related to the amount of water and fat in the tissue (Figure 2B). This indicates that it could be possible to obtain information on the composition of the tissue by using the slope of the diffuse reflectance spectra around the isosbestic points. The next step is to investigate the penetration depth at the isosbestic points to see which wavelengths are

clinically relevant for margin assessment during breast-conserving surgery.

2.2.2 | Theoretical penetration depth: Diffusion theory

To estimate the optical penetration depth of light, we used diffusion theory, which gives an approximation of the light propagation in highly scattering media [22]. The penetration depth (d_{eff}) is defined as the depth where the light fluence rate drops to $1/e$ of its initial value at the surface, and is given by [23]:

$$d_{\text{eff}} = \frac{1}{\sqrt{3\mu_a(\mu_a + \mu_s')}} \tag{1}$$

where μ_s' and μ_a respectively represent the reduced scattering and absorption coefficient. The diffuse reflectance (R_d) can also be derived from diffusion theory [24]:

$$R_d = \frac{\alpha'}{1 + 2k(1-\alpha') + \left(1 + \frac{2k}{3}\right)\sqrt{3(1-\alpha')}} \tag{2}$$

where $\alpha' = \frac{\mu_s'}{\mu_s' + \mu_a}$ and $k = \frac{1+r_d}{1-r_d}$. r_d is the internal reflection coefficient for diffuse light and depends on the refractive index of the sample, which was calculated as $n_{\text{sample}} = n_{\text{water}} + 0.14 \cdot [\text{fat}]$ [25, 26]. Where [fat] represents the fat concentration in the tissue. It can be shown that the derivative of R_d over the wavelength is:

$$\frac{dR_d}{d\lambda} = \frac{d\alpha'}{d\lambda} \cdot c \tag{3}$$

with $c = \frac{1 + 2k + \left(1 + \frac{2k}{3}\right)\sqrt{3(1-\alpha')} + \frac{(1.5+k)\alpha'}{\sqrt{3(1-\alpha')}}}{\left(1 + 2k(1-\alpha') + \left(1 + \frac{2k}{3}\right)\sqrt{3(1-\alpha')}\right)^2}$, and $\frac{d\alpha'}{d\lambda} = \frac{\mu_a \frac{d\mu_s'}{d\lambda} - \mu_s' \frac{d\mu_a}{d\lambda}}{\left(\mu_s' + \mu_a\right)^2}$. At the isosbestic points, the constant c is independent of the optical tissue properties and will not influence $\frac{dR_d}{d\lambda}$. In addition, $\mu_s' \gg \mu_a$ in tissue, and $\left|\frac{d\mu_a}{d\lambda}\right| \geq \left|\frac{d\mu_s'}{d\lambda}\right|$ in the NIR wavelength range. Therefore, $\frac{dR_d}{d\lambda}$ will be mainly shaped by the slope of the absorption spectrum and thus likely change between healthy and tumorous tissue.

We estimated the optical penetration depth and diffuse reflectance in breast tissue using known optical properties of breast tissue [13–20]. Since water and fat are the main absorbers of light in the NIR region, equations for the absorption coefficient and the reduced scattering were approximated by:

$$\mu_a(\lambda) = \varepsilon_{\text{water}}(\lambda) \cdot [\text{water}] + \varepsilon_{\text{fat}}(\lambda) \cdot [\text{fat}] \tag{4}$$

$$\mu_s'(\lambda) = \mu_{s,800}' \left(\frac{\lambda}{800\,\text{nm}}\right)^{-b} \tag{5}$$

In which [water] and [fat] represent the water and fat concentration in the tissue, and $\varepsilon_{\text{water}}$ and ε_{fat} their extinction spectra. The reduced scattering is given by the factor $\mu_{s,800}'$, which is the reduced scattering at 800 nm, and the scatter power, b. With known optical properties of breast tissue, the optical penetration depth at the isosbestic points can be estimated using Equation (1).

2.3 | Penetration depth vs imaging depth: Theory vs experiment

The penetration depth is a theoretical concept that can provide an estimate of the actual imaging depth specific to our hyperspectral setup. In this study, the imaging depth is defined as the depth required to reduce the relative reflectance by a factor of $1/e^2$. The relative reflectance is the measured reflectance divided by the maximum reflectance that could have been measured using an infinitely thick sample. Instead of $1/e^1$, which is the fluence rate at the optical penetration depth, $1/e^2$ was chosen so that the imaging depth will be similar to the penetration depth: the fluence rate of light reduces exponentially with depth, and the light travels twice the distance with the imaging depth as with the penetration depth. With the imaging depth, diffusely reflected light was measured that penetrated the tissue and was subsequently scattered back, whereas the penetration depth describes a drop in light fluence in the tissue.

To compare the theoretical penetration depth with the actual imaging depth of our hyperspectral imaging setup, we measured a tissue mimicking phantom, with known optical properties. The phantom consists of a black container that contained eight black rods with various heights (Figure 3). The rods were made of polyoxymethylene material that highly absorbs light over the whole wavelength range. The container was filled with a fat emulsion up to the height of the highest rod so that the remaining rods were covered with an emulsion layer ranging from 1 to 10 mm. The emulsion consisted of a mixture of 1 part Intralipid 20% (Fresenius, Kabi, Germany) and 19 parts deionized water. The optical properties of this emulsion were described by Aernouts et al and, with $\mu_s' = 3.8 - 8.5\,\text{cm}^{-1}$ between 900 and 1600 nm, comparable to the optical scattering properties of breast tissue [26].

The container was imaged with the hyperspectral imaging setups. To evaluate the imaging depth, nine regions of interest (ROI) were selected: eight ROIs at the position of the eight rods and one ROI in the middle of the container where the layer of fat emulsion is 30 mm and assumed effectively infinite. Second, the relative diffuse

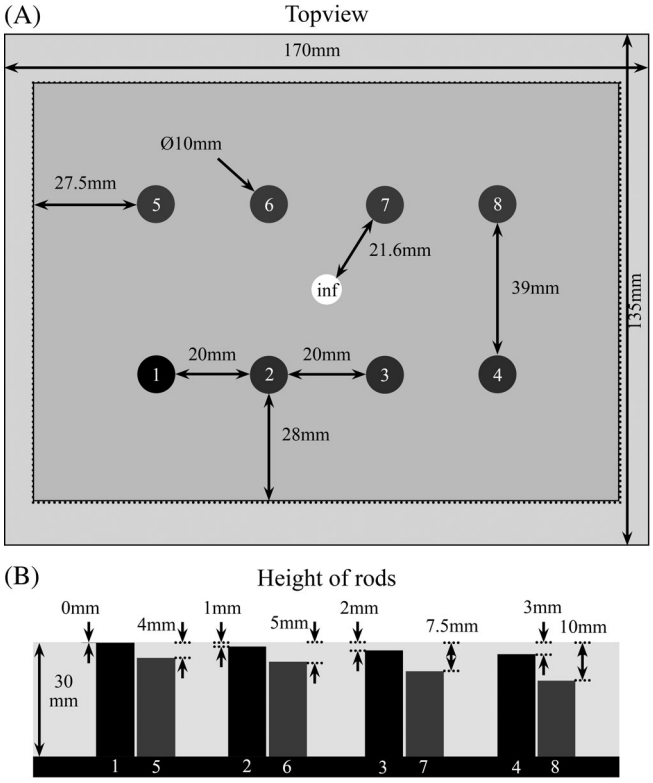

FIGURE 3 (A) Schematic view of the phantom. In the container, 8 rods with different heights are placed on a plate of polymethylene. Subsequently, the container is filled with a fat emulsion up to the height of the highest rod (rod 1), so that the remaining rods were covered with a fat emulsion layer ranging from 1 to 10 mm (B). "inf" indicates the region of interest of the infinite fat emulsion layer

reflectance (R_{rel}) was calculated for the ROIs at the rods. This is the diffuse reflectance, relative to the diffuse reflectance measured at the infinite fat emulsion layer. By plotting this R_{rel} against the layer thickness (d) above each rod, we expect an exponential curve similar to the exponential curve describing the decrease of diffuse light in highly scattering tissue with depth [22]. This curve can be described by:

$$R_{rel}(\lambda,d) = 1 - f_1 e^{-f_2 d} \tag{6}$$

where f_1 and f_2 are the variables that are fitted to the data using the nonlinear least-squares solver in Matlab 2018a (The Math Works Inc., Natick, Massachusetts, USA). As mentioned before, we defined the imaging depth as the depth at which R_{rel} equals $1\text{-}1/e^2$.

2.4 | Classification method: Spectral slope method

In Section 2.2.1, we hypothesized that the slope of the reflectance spectrum around the isosbestic point could be used to discriminate between healthy and tumor tissue. Therefore, we calculated the first order derivative, the spectral slope, from the diffuse reflectance spectra obtained on breast specimens, at each isosbestic point using the following equation:

$$\frac{dR_d(\lambda_0)}{d\lambda} = \frac{R_d(\lambda+\Delta\lambda) - R_d(\lambda-\Delta\lambda)}{2\cdot\Delta\lambda} \tag{7}$$

Where $\frac{dR_d(\lambda_0)}{d\lambda}$ is the spectral slope at the isosbestic point (λ_0), R_d the diffuse reflectance and λ the wavelength band in millimeter. The spectral slope was calculated by choosing two wavelengths, each at a distance $\Delta\lambda$ from the isosbestic point.

The optimal distance, $\Delta\lambda$, for the spectral slope method should meet two requirements. First, this distance should be as small as possible to prevent large penetration depth variations within the wavelength range with tissue composition. Second, $\Delta\lambda$ should be large enough to use the spectral slope to predict the amount of fat in the tissue, that is, obtain detectable differences between tumor and healthy tissue. The relation between the spectral slope and the amount of fat was expected to be linear and therefore analyzed using the Pearson correlation coefficient (PCC). An absolute PCC of 1 indicates a perfect linear correlation, whereas a PCC of 0 indicates no correlation. The minimum $\Delta\lambda$ that has to be used for the spectral slope depends on the signal-to-noise ratio (SNR) of the hyperspectral camera since a smaller $\Delta\lambda$ is more likely to generate a nosier slope. Therefore, white noise was added to the estimated reflectance spectra up to a maximum that corresponded to an SNR of 50, which was the minimum SNR of the cameras at the isosbestic points. We selected the optimal $\Delta\lambda$ based on two requirements. First, the variation in penetration depth should not exceed 20% of the penetration depth at the isosbestic point. Second, for all different amounts of added noise, the PCC should be highest.

2.5 | Applying classification method to breast specimens

To evaluate whether the spectral slope at the isosbestic points can differentiate between healthy and tumor tissue, the method was applied to ex vivo breast samples. This study was approved by the Institutional Review Board of the Netherlands Cancer Institute/Antoni van Leeuwenhoek. According to Dutch law (WMO), no written informed consent from patients was required. Fresh surgical specimens were obtained from female patients undergoing primary breast surgery at the Antoni van Leeuwenhoek hospital. Immediately after resection, the breast specimen was

brought to the pathology department. There the specimen was inked and subsequently sliced in 2 to 6 mm thick tissue slices, according to standard histopathologic procedure. One tissue slice was placed in a macrocassette on top of black rubber and used for the optical measurements. The black rubber highly absorbs light from 400 to 1700 nm and prevents that any other underlying structure under the tissue is measured. The optical measurements were performed within 10 minutes after collection of the tissue at the pathology department.

After a few days, the tissue slices were processed in H&E stained sections according to standard protocol. These sections were registered to the hyperspectral images using a white light image that was taken simultaneously to the hyperspectral image and a non-rigid registration algorithm. This process is described in our earlier publication [7]. After registering the annotated H&E section to the hyperspectral image, the whole hyperspectral image was annotated with tissue types being invasive carcinoma (IC), adipose tissue and connective tissue. To exclude potential histopathology registration errors, only areas 1 mm away from a tissue class border were selected for the evaluation of the spectral slope method.

From 19 patients, one slice per patient was measured with a mean slice thickness of 3.7 mm (range 2.5-5.5 mm). Table 1 shows the characteristics of the patients, the tissue slices and the tumor. The age of these patients was 61 ± 11 years (mean ± SD), and their ACR score, which reflects the breast density and ranges from 1 (low breast density) to 4 (high breast density), was 2.68 ± 0.74 (mean ± SD). The type and grade of IC varied between the 19 patients: 4, 12 and 1 patient contained invasive ductal carcinoma (IDC) grade I, grade II and grade III respectively. The other two patients contained invasive lobular carcinoma grade II and III. Difference between the spectral slope in tumor and healthy tissue were evaluated for each patient individually using a non-parametric Kruskal-Wallis test [27], and over all patients using a two-level hierarchical model with the repeated measurements per patient in level one, and the tissue type in level two. P values <.05 were considered statistically significant.

3 | RESULTS AND DISCUSSION

3.1 | Results

3.1.1 | Theoretical penetration depth in breast tissue

Figure 4 shows the diffuse reflectance and optical penetration depth in human breast tissue for different optical

TABLE 1 Characteristics of patients, slices and tumor

	Patient characteristics			Tumor characteristics	
Patient #	Age	ACR score	Slice thickness (mm)	Type	Grade
1	57	1	3	IDC	3
2	77	2	4.5	ILC	3
3	74	2	3	IDC	2
4	54	3	5.5	ILC	2
5	49	3	3.5	IDC	2
6	73	4	2.5	IDC	1
7	51	4	3	IDC	2
8	57	2	2.5	IDC	1
9	77	3	3	IDC	1
10	63	2	4.5	IDC	2
11	68	3	4.5	IDC	2
12	48	2	4	IDC	2
13	58	3	4	IDC	1
14	67	2	2.5	IDC	2
15	53	3	2.5	IDC	2
16	73	3	4	IDC	2
17	57	3	4.5	IDC	2
18	51	3	5	IDC	2
19	43	3	5	IDC	2

Abbreviations: IDC, invasive ductal carcinoma; ILC, invasive lobular carcinoma.

properties, as estimated using Equation (2). The green arrows indicate the isosbestic points of the water and fat extinction coefficients at which the optical penetration depth does not depend upon the tissue properties. The optical penetration depth around these points differs: for example, around 930 and 1200 nm, the light penetrates the breast tissue up to approximately 6.5 and 2 mm, respectively, whereas above 1700 nm imaging is more superficial. Given the preferred tumor-free margin width of 2 mm, the isosbestic points around 1200 nm are clinically most relevant for resection margin assessment during breast-conserving surgery [3].

3.1.2 | Penetration depth vs imaging depth: Theory vs experiment

Figure 5 shows the comparison between the estimated penetration depth and the experimentally obtained imaging depth of our hyperspectral system. Figure 5B,C show the hyperspectral images of the tissue-mimicking phantom for two of the four isosbestic points within the wavelength range of our cameras. More of the deeper situated rods were visible in the image at 931 nm, which indicates that the imaging depth in the fat emulsion is higher at 931 nm than at 1197 nm. Figure 5D shows the spectra of an infinite fat emulsion layer as measured with the hyperspectral camera (black dotted line) and estimated with diffusion theory (red dotted line). The spectra were comparable, with only a small difference (less than 2.5%) between the estimated and measured spectra above 1150 nm.

In addition, Figure 5D shows the averaged diffuse reflectance spectra measured at the ROI of each rod. For shorter wavelengths, the imaging depth was larger (Figure 5E). Therefore, larger layer thicknesses were required for the diffuse reflectance to be identical to the measured infinite layer. Table 2 shows the penetration depth and the imaging depth at the isosbestic points. In general, the measured imaging depth was lower than the estimated penetration depth, especially at 910 and 931 nm. The theoretical penetration depth around 1200 nm in the phantom was slightly lower than the theoretical penetration depth in breast tissue: at 1197 nm 1.91 mm vs 2.01 ± 0.22 mm and at 1222 nm 2.00 mm vs 2.14 ± 0.26 mm. Therefore, we expect the imaging depth of our hyperspectral setup in breast tissue to be slightly higher than the imaging depth in the fat emulsion as well.

3.1.3 | Classification method: Spectral slope method

Around 1200 nm, two isosbestic points are located: 1197 and 1222 nm. We optimized the distance $\Delta\lambda$ around these two points to minimize differences in penetration depth for different water/fat concentrations, while allowing for good differentiation between tumor and healthy tissue. Based on this analysis, 1197 nm allowed for the best tissue discrimination with minimal penetration depth variations. As shown in Figure 6, the optimal distance $\Delta\lambda$ around this isosbestic point was 10 nm.

Figure 7 shows the spectral slope around 1197 nm, calculated with the optimal $\Delta\lambda$, for different fat concentrations. With this spectral slope, the fat percentage in the tissue can be estimated. The variations in the boxplots are induced by variations in the reduced scattering we used and increase with the fat percentage. In breast tissue, the reduced scattering is unknown and varies from patient to patient. Therefore, the accuracy of the estimated fat percentage will be lower when the actual fat percentage in the tissue is higher.

3.1.4 | Applying classification method to breast specimens

The spectral slope method was applied to ex vivo breast samples to evaluate whether healthy and tumor tissue could be distinguished. Figure 8 shows the average diffuse reflectance spectra per tissue type. In comparison

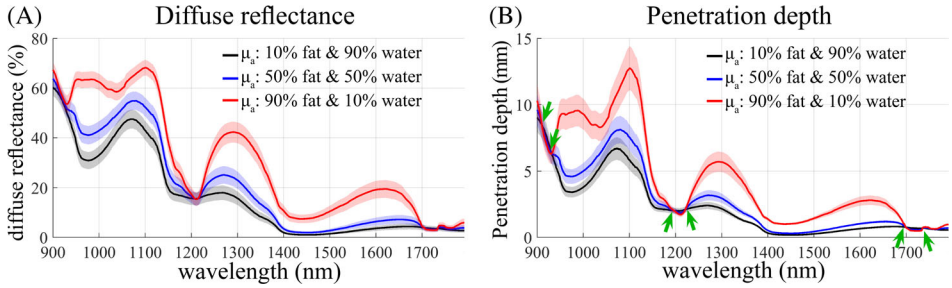

FIGURE 4 The diffuse reflectance (A) and penetration depth (B) for three fat-water concentrations and a reduced scattering that varied due to differences in the factor $\mu'_{s,\,800}$ (5-10 mm^{-1}) and the scatter power (0.5-1.25). The shaded areas around the graphs depict the SD due to variation in reduced scattering. The green arrows indicate wavelength regions at which the penetration depth of the photons did not depend upon the tissue properties, that is, the isosbestic points of the water and fat absorption coefficients

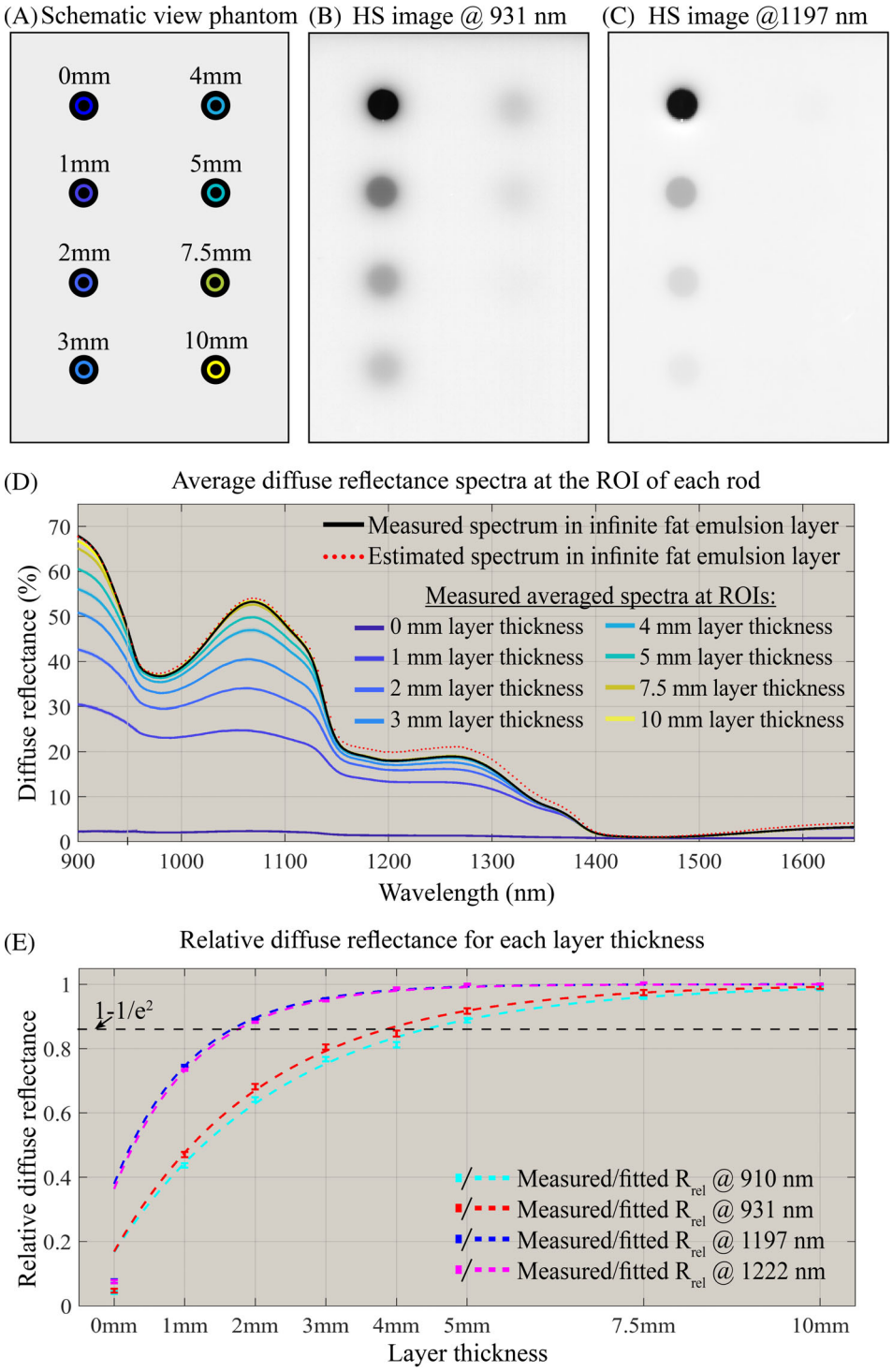

FIGURE 5 The schematic view (A) and the hyperspectral (HS) image of the tissue mimicking phantom at two of the four isosbestic points (B and C) within the wavelength range of our cameras. The colored circles in the rods (A) represent the ROIs of each rod. The shown spectra (D, colormap: parula) are the averaged diffuse reflectance spectra at these ROIs. The layer thicknesses of the fat emulsion above the rods varies. In addition, the measured and estimated spectra of an infinite fat emulsion layer are shown. By plotting the relative diffuse reflectance at the ROIs against the layer thickness of the fat emulsion (E), the imaging depth of light can be calculated at the isosbestic points

with the estimated diffuse reflectance (gray values), the measured diffuse reflectance was in the same range at the isosbestic points around 1200 nm, but much lower around 930 nm. This deviation was caused by the thickness of the tissue slices with respect to the optical penetration depth in tissue (Figure 4). Since light around 930 nm has a penetration depth of approximately 6.5 mm, it penetrates through tissue with a thickness of 5.5 mm. Therefore, it was partly absorbed by the rubber underneath the tissue, and less light was diffusely reflected and collected by the camera. Figure 8B,C show that the thicker a slice, the more the measured reflectance resembled the estimated reflectance.

Figure 9 shows a boxplot of the spectral slope at 1197 nm per tissue type for each patient sample. The median spectral slope of IC was significantly different from adipose tissue ($P < .0001$) in all patients and significantly different from connective tissue ($P < .0001$) in 11 of the 13 patients.

TABLE 2 Estimated theoretical penetration depth using diffusion theory and measured imaging depth of our hyperspectral imaging setup in the fat emulsion

Isosbestic points (nm)	Theoretical penetration depth according to diffusion theory (mm)[a]	Measured imaging depth of our hyperspectral setup (mm, mean ± SD)[b]
910	7.38	4.49 ± 0.14
931	5.56	3.92 ± 0.15
1197	1.91	1.71 ± 0.02
1222	2.00	1.79 ± 0.03
1699	0.79	Not available
1735	0.73	Not available

[a]The depth required to reduce the fluence rate by a factor of $1/e^1$.
[b]The depth required to reduce the relative reflectance by a factor of $1/e^2$.

The linear correlation between the ACR score of the patient and the spectral slope at 1197 was calculated with the Pearson Correlation Coefficient en was for IC, adipose tissue and connective tissue respectively −0.26, −0.07 and −0.53. Therefore, in patients with a higher ACR score, the spectral slope around 1197 nm was higher in IC and connective tissue, and therefore the fat percentage was lower. Over all patients, statistical analysis revealed that the spectral slope of IC was significantly different from both connective tissue ($P = .043$) and adipose tissue ($P < .001$). Since the spectral slope of IC was on average higher than the spectral slope of both adipose (by 1.257) and connective tissue (by 0.122), IC contained on average less fat than the two healthy tissue types.

3.2 | Discussion

In this study, we developed a method that allows for hyperspectral analysis of resection margins in breast cancer, while imaging up to a depth similar to the required tumor-free margin width of 2 mm. We used diffusion theory to estimate the optical penetration depth and compare this with experimentally obtained data. Since the penetration depth cannot be measured directly from reflectance measurements, we measured the imaging depth specific to our setup and defined this imaging depth to be similar to the penetration depth. However, the measured imaging depth was lower than the estimated penetration depth, especially at wavelengths with higher penetration depths (Table 2 and Figure 5). This was related to our measurement setup, where the imaged scene was illuminated under an angle of 45°, to reduce the amount of specular reflection in the measurements. Previous research showed that the illumination of a medium at an oblique angle shifts the center of the diffuse reflectance away from the incident point [28, 29]. Thereby, the imaging depth can decrease with the angle of illumination incidence. Equation (2), however, purely describes the penetration of collimated light through an optically homogeneous medium without taking into account any properties of the measurement setup. As a result, the imaging depth can be much lower than the penetration depth, especially for wavelengths with higher penetration depths, such as 910 and 931 nm. Diffusion theory can thus provide an estimate of the imaging depth, but if a more precise estimate is needed for a specific measurement setup, measuring the imaging depth with a phantom is useful.

In addition, we verified with the phantom that estimating the diffuse reflectance with diffusion theory was representative for the diffuse reflectance measured with the hyperspectral camera. Despite small differences above 1150 nm (Figure 5D), which were resolved when adapting the assumed scattering properties, the spectra were comparable [26]. Adaptations to these scattering properties were minimal (10%) and most likely needed to compensate for the layering of Intralipid, as described by Bodenschatz et al, and its

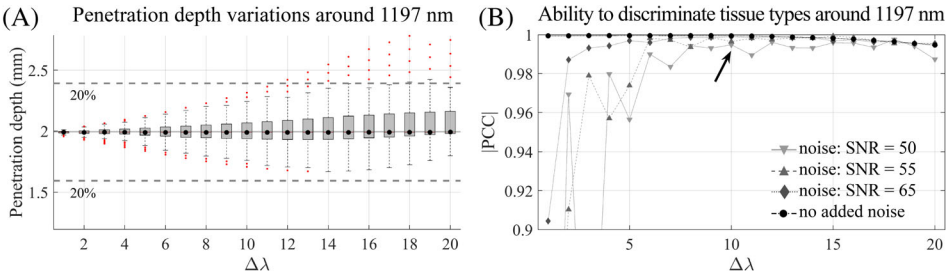

FIGURE 6 Selection of the optimal $\Delta\lambda$ around the isosbestic point 1197 nm. (A) illustrates the increase in penetration depth variations with an increase in $\Delta\lambda$. The red dots represent the outliers in the boxplots. The penetration depth in this figure was estimated using 11 different water/fat concentrations, from 0% fat and 100% water to 100% fat and 0% water, and a reduced scattering of $7.5\left(\frac{\lambda}{800\,\text{nm}}\right)^{-0.875}$. The same optical properties were used in (B), which shows which $\Delta\lambda$ allows for the best tissue discrimination, that is, how well the spectral slope can be used to predict the amount of fat in the tissue. The spectral slope is expected to be linear related to the amount of fat in the tissue and analyzed using the absolute Pearson correlation coefficient (PCC). The arrow points at the |PCC| corresponding to the selected optimal $\Delta\lambda$ of 10 nm

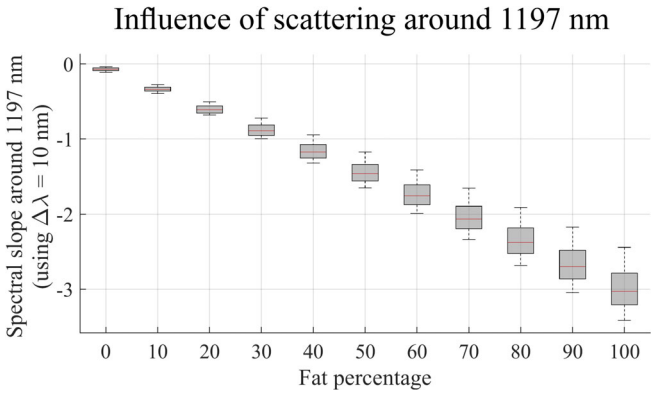

FIGURE 7 Influence of the scattering on the spectral slope method. The spectral slope around the isosbestic points is calculated for different water/fat concentration using the optimal $\Delta\lambda$. Variations in the boxplots are related to different scattering properties, which varied due to differences in the factor $\mu'_{s,\,800}$ (5-10 mm^{-1}) and the scatter power (0.5-1.25)

potentially induced error for surface sensitive techniques [30].

With diffusion theory, we also estimated the optical penetration depth in human breast tissue. For clinical measurements, well-substantiated information on this depth is important. First, for tissue discrimination with hyperspectral imaging, it is important to take into account the influence of the thickness of tissue slices on the measured reflectance. As visualized in both the phantom (Figure 5D) and the breast tissue slices (Figure 8), when light penetrates through a medium that is thinner than the optical penetration depth, spectra will be altered by the material underneath the medium. As a result, for data analysis, the slice thickness might influence the classification result. Second, for hyperspectral imaging in the clinical setting, knowledge on the assessed margin width is important. For resection margin assessment, the American clinical guideline requires a tumor-free resection surface for IC and a tumor-free margin width of 2 mm for its (potential) precursor ductal carcinoma in situ (DCIS) [3]. Therefore, hyperspectral margin assessment should only assess tissue up to 2 mm underneath the resection surface. With our cameras, the minimum optical penetration depth at the isosbestic points was approximately 2 mm. For hyperspectral imaging in the clinical setting, this is sufficient for DCIS, but deeper than necessary for IC. Based on diffusion theory, higher wavelength regions, for example around 1715 nm, might provide a solution for more superficial imaging. However, since our current hyperspectral camera was limited to 1646 nm, we were not able to include this region in our analysis.

The results of the spectral slope method to differentiate healthy and tumor tissue in ex vivo breast tissue slices are promising. Even though we observed an inter-patient variability related to the patients' breast density, as has been reported by other research as well [14, 31], the spectral slope at 1197 of IC was significantly different from healthy tissue in 11 of the 13 patients. In addition, over all patients, the spectral slope in tumor was significantly different from healthy tissue. For this, only two wavelengths, instead of the whole spectrum, were required. This offers great potential for improvement of the current imaging setup: currently, hyperspectral data is captured by moving the imaged scene,

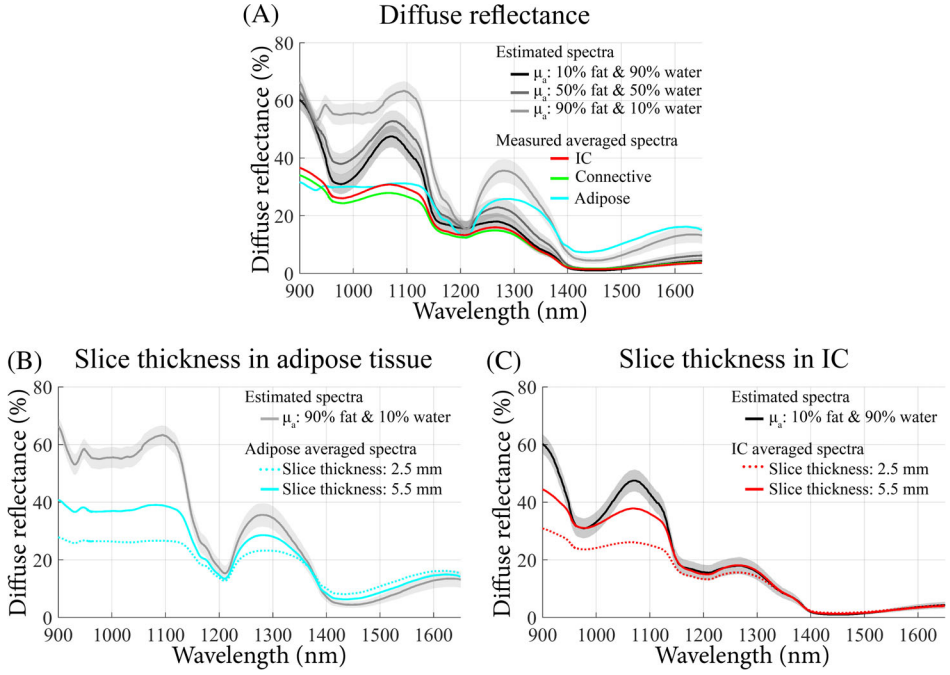

FIGURE 8 (A) Average measured diffuse reflectance spectra of invasive carcinoma (IC), connective and adipose tissue. The estimated diffuse reflectance spectra (gray values) correspond to the spectra shown in Figure 4. The difference between the measured and estimated reflectance is the result of the thickness of the tissue slices with respect to the penetration depth. (B and C) show the influence of the thickness of the tissue slices in both adipose tissue and IC

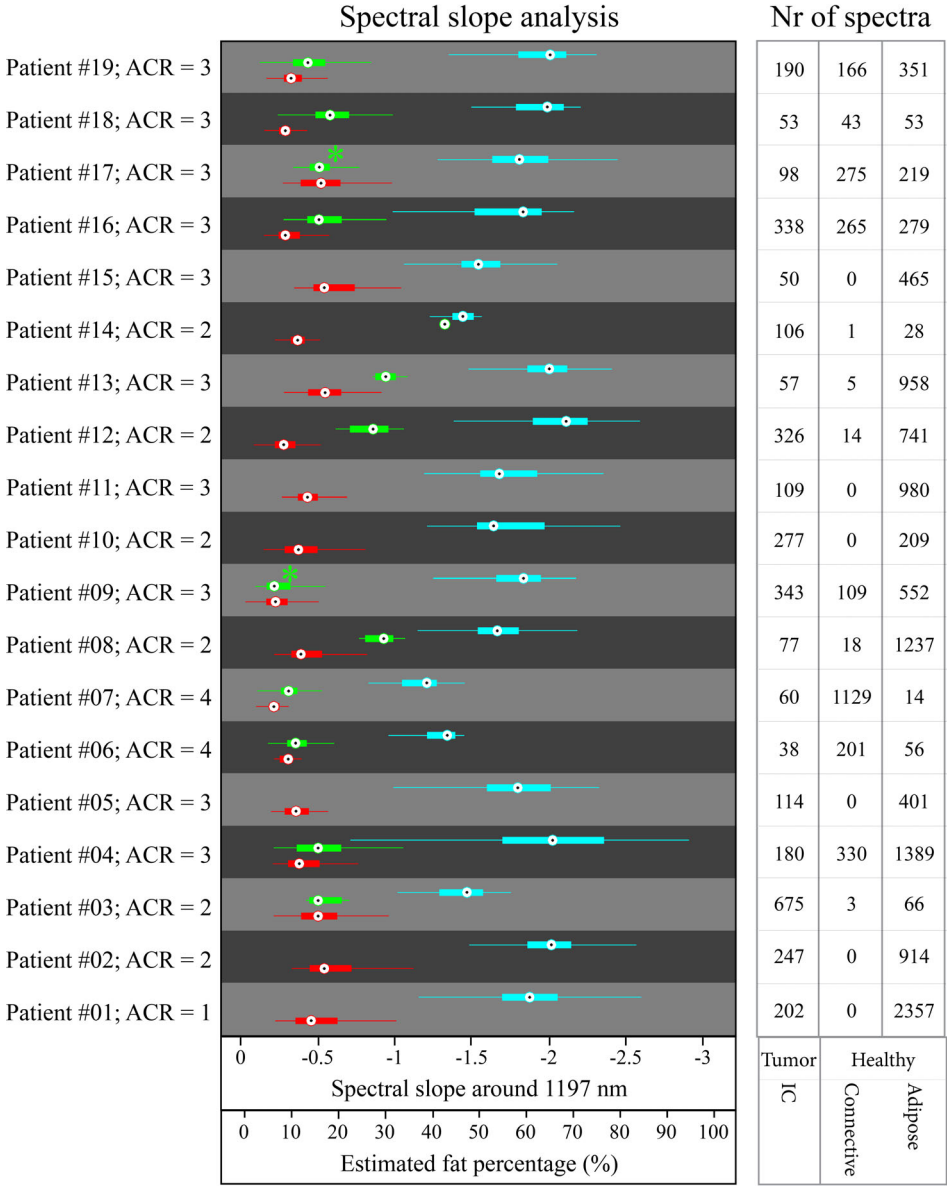

FIGURE 9 Spectral slope analysis of breast tissue at 1197 nm. The ACR score reflects the breast density. Tissue types are invasive carcinoma (IC, red), connective (green) and adipose tissue (cyan). The fat percentage was estimated using the graph of Figure 7, and the spectral slope. The two asterisks indicate no significant difference in the spectral slope between IC and connective tissue (patient #9, $P = .5082$; patient #17, $P = .2997$)

which makes the system impractical for in vivo imaging. By reducing the number of spectral bands, a stationary multispectral imaging system can be developed that will be less expensive, image faster and might be more practical in vivo. To make a more solid statement on the performance of the spectral slope method for intra-operative resection margin assessment, that is, validate if the spectral slope method allows for tumor detection up to the required tumor-free margin width, we will perform a clinical study in the future that measures and analyzes the resection margin of lumpectomy specimens using this technique.

In this paper, we focused on breast cancer, but the same approach can be used to develop a resection margin assessment method for other types of cancer. Based on the tissue properties and required tumor-free margin width, the same strategy can be used to identify optimal wavelengths that can be used to discriminate healthy from tumor tissue.

4 | CONCLUSION

Hyperspectral imaging is a promising technique for intra-operative margin assessment during cancer surgery. In this study, we developed a method, based on the spectral slope, that allows for hyperspectral analysis of resection margins in breast cancer. While imaging up to a depth similar to the required tumor-free margin width of 2 mm, this method can discriminate between healthy and tumor tissue. In this paper, we focused on breast cancer, but the same approach can be applied to develop a method for other types of cancer.

ACKNOWLEDGMENTS

The authors gratefully acknowledge the financial support of this research by the KWF Kankerbestrijding (grant KWF 10747). The authors thank the NKI-AVL core Facility

Molecular Pathology & Biobanking (CFMPB) for supplying NKI-AVL biobank material and all pathologist assistants from the Department of Pathology and all surgeons and nurses from the Department of Surgery for their assistance in collecting the specimens.

ORCID

Esther Kho https://orcid.org/0000-0001-9783-1588

REFERENCES

[1] R. W. Smits, S. Koljenović, J. A. Hardillo, I. Ten Hove, C. A. Meeuwis, A. Sewnaik, E. A. Dronkers, T. C. Bakker Schut, T. P. Langeveld, J. J. H. Molenaar, and neck, *Head Neck*. **2016**, *38*, E2197.

[2] D. Mukkai Krishnamurty, P. E. J. Wise, *J. Surg. Oncol.* **2016**, *113*, 323.

[3] S. G. Brouwer de Koning, M. T. F. D. Vrancken Peeters, K. Jóźwiak, P. A. Bhairosing, T. J. M. Ruers, *Clin. Breast Cancer* **2018**, *18*, 595.

[4] G. Lu, B. Fei, *J. Biomed. Opt.* **2014**, *19*, 010901.

[5] G. Lu, D. Wang, X. Qin, S. Muller, X. Wang, A. Y. Chen, Z. G. Chen, B. Fei, *J. Biophotonics* **2017**, *11*, e201700078.

[6] H. Akbari, K. Uto, Y. Kosugi, K. Kojima, N. Tanaka, *Cancer Sci.* **2011**, *102*, 852.

[7] E. Kho, L. L. de Boer, K. K. Van de Vijver, F. van Duijnhoven, M.-J. T. F. D. Vrancken Peeters, H. J. C. M. Sterenborg, T. J. M. Ruers, *Clin. Cancer Res.* **2019**, *25*, 3572.

[8] A. M. Hosking, B. J. Coakley, D. Chang, F. Talebi-Liasi, S. Lish, S. W. Lee, A. M. Zong, I. Moore, J. Browning, S. L. Jacques, and medicine, *Lasers Surg. Med.* **2019**, *51*, 214.

[9] A. O. Gerstner, W. Laffers, F. Bootz, D. L. Farkas, R. Martin, J. Bendix, B. J. J. o. B. Thies, *J. Biophotonics* **2012**, *5*, 255.

[10] L. L. Randeberg, E. L. Larsen, L. O. Svaasand, *SPIE BiOS, Photonic Therapeutics and Diagnostics V*, Vol. 7161, International Society for Optics and Photonics, San Jose, California, USA; **2009**.

[11] H. Zhang, D. C. Salo, D. M. Kim, S. Komarov, Y.-C. Tai, M. Y. Berezin, *J. Biomed. Opt.* **2016**, *21*, 126006.

[12] A. Bjorgan, M. Milanic, L. L. Randeberg, *J. Biomed. Opt.* **2014**, *19*, 066003.

[13] A. Cerussi, N. Shah, D. Hsiang, A. Durkin, J. Butler, B. J. Tromberg, *J. Biomed. Opt.* **2006**, *11*, 044005.

[14] L. L. de Boer, B. Molenkamp, T. M. Bydlon, B. H. W. Hendriks, J. Wesseling, H. J. C. M. Sterenborg, T. J. M. Ruers, *Breast Cancer Res. Treat.* **2015**, *152*, 509.

[15] P. G. Anderson, J. M. Kainerstorfer, A. Sassaroli, N. Krishnamurthy, M. J. Homer, R. A. Graham, S. Fantini, *PLoS One* **2015**, *10*, e0117322.

[16] A. Leproux, A. Durkin, M. Compton, A. E. Cerussi, E. Gratton, B. J. Tromberg, *Breast Cancer Res.* **2013**, *15*, R89.

[17] R. Nachabé, D. J. Evers, B. H. Hendriks, G. W. Lucassen, M. van der Voort, E. J. Rutgers, M.-J. V. Peeters, J. A. Van der Hage, H. S. Oldenburg, J. Wesseling, *J. Biomed. Opt.* **2011**, *16*, 087010.

[18] D. B. Jakubowski, A. E. Cerussi, F. P. Bevilacqua, N. Shah, D. Hsiang, J. A. Butler, B. J. Tromberg, *J. Biomed. Opt.* **2004**, *9*, 230.

[19] S. L. Jacques, *Phys. Med. Biol.* **2013**, *58*, R37.

[20] S. Fantini, A. Sassaroli, *Ann. Biomed. Eng.* **2012**, *40*, 398.

[21] R. Nachabé, B. H. Hendriks, A. E. Desjardins, M. van der Voort, M. B. van der Mark, and H. J. Sterenborg, *J. Biomed. Opt.* **2010**, *15*, 037015.

[22] A. J. Welch, M. J. C. van Gemert, *Optical-Thermal Response of Laser-Irradiated Tissue*, Springer, Dordrecht, the Netherlands **2011**, p. 145.

[23] B. C. Wilson, S. L. Jacques, *IEEE J. Quantum Elect.* **1990**, *26*, 2186.

[24] S. T. Flock, M. S. Patterson, B. C. Wilson, D. R. Wyman, *I.E.E. E. Trans. Biomed. Eng.* **1989**, *36*, 1162.

[25] R. Groenhuis, H. A. Ferwerda, J. Ten Bosch, *Appl. Optics* **1983**, *22*, 2456.

[26] B. Aernouts, R. Van Beers, R. Watté, J. Lammertyn, W. Saeys, *Opt. Express* **2014**, *22*, 6086.

[27] W. H. Kruskal, W. A. Wallis, *J. Am. Stat. Assoc.* **1952**, *47*, 583.

[28] L. Wang, S. L. Jacques, *Appl. Optics* **1995**, *34*, 2362.

[29] P. Lai, X. Xu, L. V. Wang, *J. Biomed. Opt.* **2014**, *19*, 035002.

[30] N. Bodenschatz, P. Krauter, F. Foschum, S. Nothelfer, A. Liemert, E. Simon, S. Kröner, A. Kienle, *Phys. Med. Biol.* **2015**, *60*, 1171.

[31] J. Wang, S. Jiang, Z. Li, R. M. diFlorio-Alexander, R. J. Barth, P. A. Kaufman, B. W. Pogue, K. D. Paulsen, *Med. Phys.* **2010**, *37*, 3715.

SUPPORTING INFORMATION

Additional supporting information may be found online in the Supporting Information section at the end of this article.

How to cite this article: Kho E, de Boer LL, Post AL, et al. Imaging depth variations in hyperspectral imaging: Development of a method to detect tumor up to the required tumor-free margin width. *J. Biophotonics*. 2019;e201900086. https://doi.org/10.1002/jbio.201900086